Ref. Ares(2025)6330046 - 04/08/2025

Tech UPGRADE

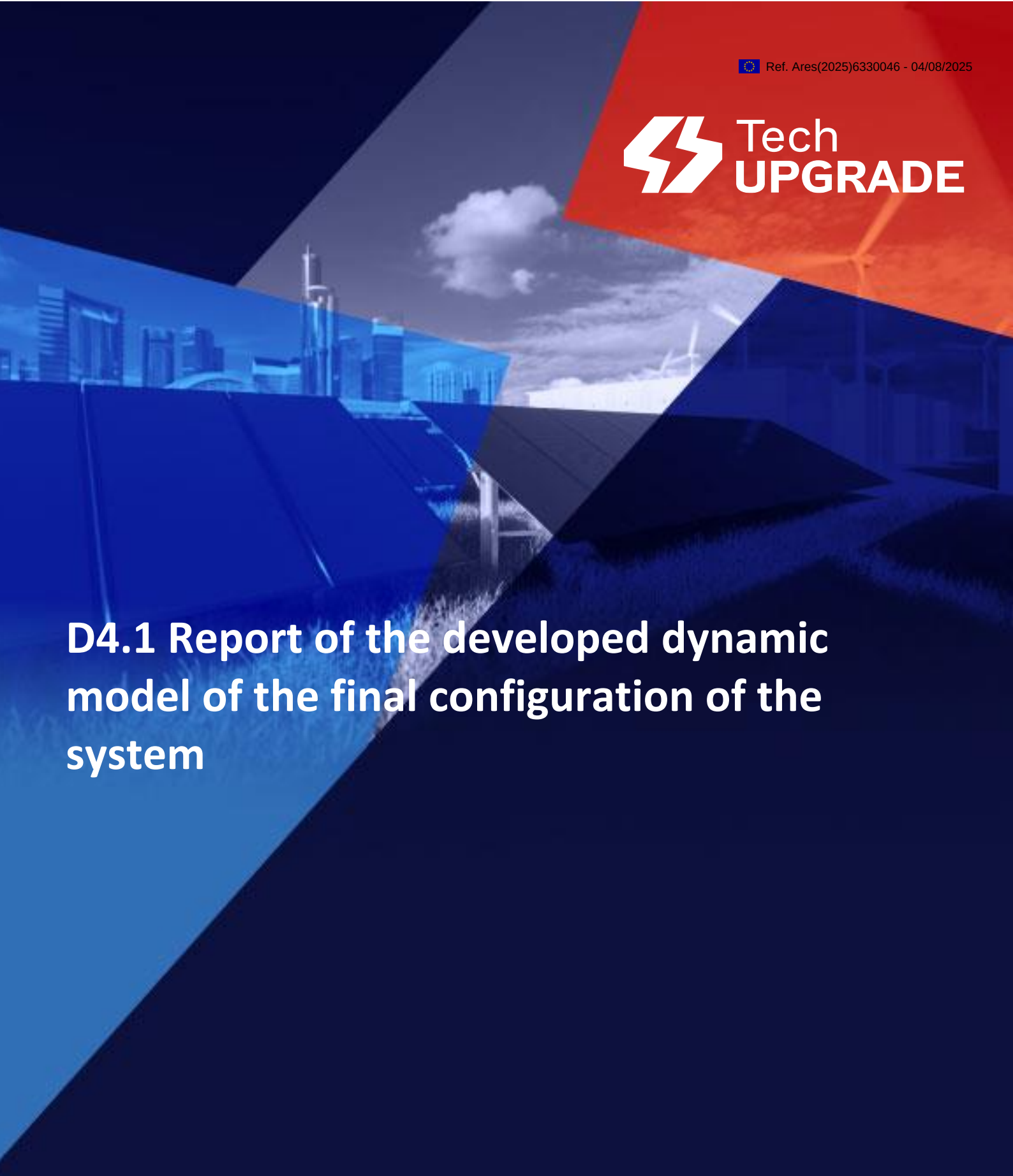

D4.1 Report of the developed dynamic model of the final configuration of the system

Funded by the European Union

This project has received funding from European Union's Horizon Europe's Research and Innovation Program under grant agreement No. 101103966. Views and opinions expressed are however those of the author(s) only and do not necessarily reflect those of the European Union or the European Climate, Infrastructure and Environment Executive Agency (CINEA). Neither the European Union nor the granting authority can be held responsible for them.

Deliverable 4.1 Report of the developed dynamic model of the final configuration of the system

Actual Submission Date: **31/07/2025**

Produced by: **DTU- Nabat, Mohammad Hossein**

TechUPGRADE

techupgrade.eu

HORIZON-CL5-2022-D4-01

Thermochemical Heat Recovery and Upgrade for Industrial Processes

Grant Agreement no.: 101103966

Start date of project: 1 May 2023 - Duration: 48 months

DELIVERABLE FACTSHEET

Deliverable D2.3	
Nature of the Deliverable:	R— Document, report
Due date of the Deliverable:	M27 – 31/07/2025
Actual Submission Date:	M27 – 31/07/2025
Produced by:	DTU- Mohammad Hosein Nabat
Contributors:	Hamid Reza Rahbari, Ahmad Arabkoohsar
Work Package Leader	DTU – Ahmad Arabkoohsar
Reviewed by:	DTU- Hamid Reza Rahbari

Dissemination level	
X	PU = Public
	PP = Restricted to other programme participants (including the EC)
	RE = Restricted to a group of the consortium (including the EC)
	CO = Confidential, only members of the consortium (including the EC)

Contents

Figures

Tables

1 Summary

This deliverable presents the dynamic model developed for the final configuration of the TechUPGRADE project's system, which is a solid-gas thermochemical heat transformer (SGTHT). The model is simulated in Dymola software using Modelica and the TIL library. This dynamic model predicts the transient behavior of the system during both hydration and dehydration reactors. The energy balance, reaction kinetics, and thermal resistance of the coupled heat and mass transfer equations between the salt bed and the heat transfer fluid (HTF) are considered in this model. This model is validated using experimental data from previous studies. The validation shows a good compromise with the temperature profile, reaction rate, and thermal power. However, due to the lump-parameter approach, there are deviations. The results show that the vapor pressure and the mass flow rate of HTF have a significant impact on the performance of the system. Future work will focus on developing a one-dimensional model to improve accuracy and correct the dynamic reactor response.

2 Introduction

The demand for energy in the industry is continuously increasing, and fossil fuels are still the main source of supply. However, a significant portion of the energy consumed is wasted as heat. Therefore, heat recovery is very important for increasing industry sector sustainability and reducing environmental pollution. Current heat recovery technologies are unable to recover all the waste heat. Additionally, the mismatch between the temperature of waste heat and industrial demand has made thermochemical heat transfer (THT) systems a promising solution for recovering and upgrading waste heat to usable temperatures. Among various types of THT, the solid-gas thermochemical heat transformer (SGTHT) system offers notable advantages such as high energy density and scalability [1].

The SGTHT systems operate based on solid-gas reversible chemical reactions. During the dehydration process, chemical bonds are decomposed inside the salt, releasing water vapor and storing waste heat through a heating reaction (dehydration process). During the hydration process, the water vapour at a higher temperature enters the dehydrated salt, reversing the process, and releases the stored thermal energy by restoring chemical bonds. By adjusting the vapor pressure, the temperature at which heat is released can be precisely controlled, enabling SGTHT systems to serve as a flexible solution to heat recovery.

In recent years, many studies were done in this field. For example, Malleshwar et al. [2] examined the performance of an SGTHT system in recovering waste heat from high-temperature heat pumps. They proposed various configurations based on the K_2CO_3 salt and demonstrated that the system could achieve a thermal efficiency of 85.3%. Michel et al. [3] experimentally showed that using $CaCl_2$ salt could increase the recovered heat by 60°C. Through a series of experimental and numerical studies, Stengler et al. [4–6] demonstrated that strontium bromide monohydrate ($SrBr_2{\cdot}H_2O$) can raise waste heat temperatures by 100°C. In addition, the high performance of the reactor used enables the recovery of waste heat and efficient upgrade. Michelle et al. [7] examined the performance of the SGTHT system with various salts. They found that $SrBr_2$ and $CaCl_2$ provide better performance and temperature lift than other salts.

Given the importance and advantages of SGTHT systems, the present study dynamically models an $SrBr_2{\cdot}H_2O$-based SGTHT system. This dynamic analysis enables us to examine how the temperatures of the salt and heat transfer fluid (HTF) change during heat recovery and upgrading operations, and to analyze the rate of heat recovery and temperature increase with respect to pressure and time.

3 Dynamic Modeling of the SGTHT System

Dynamic modeling of the SGTHT system is carried out using the Modelica language and the TIL library within the Dymola simulation environment. This approach enables analysis of transient behavior and facilitates the investigation of the effects of key process variables on system performance.

3.1 Reactor Model

The overall schematic of the developed model for dynamic reactor simulation is shown in Figure 1. The model structure comprises two main control volumes: one for the hydrated salt and another for the HTF, which facilitates heat exchange to and from the reactor. To accurately represent heat transfer between these control volumes, a set of thermal resistances has been defined.

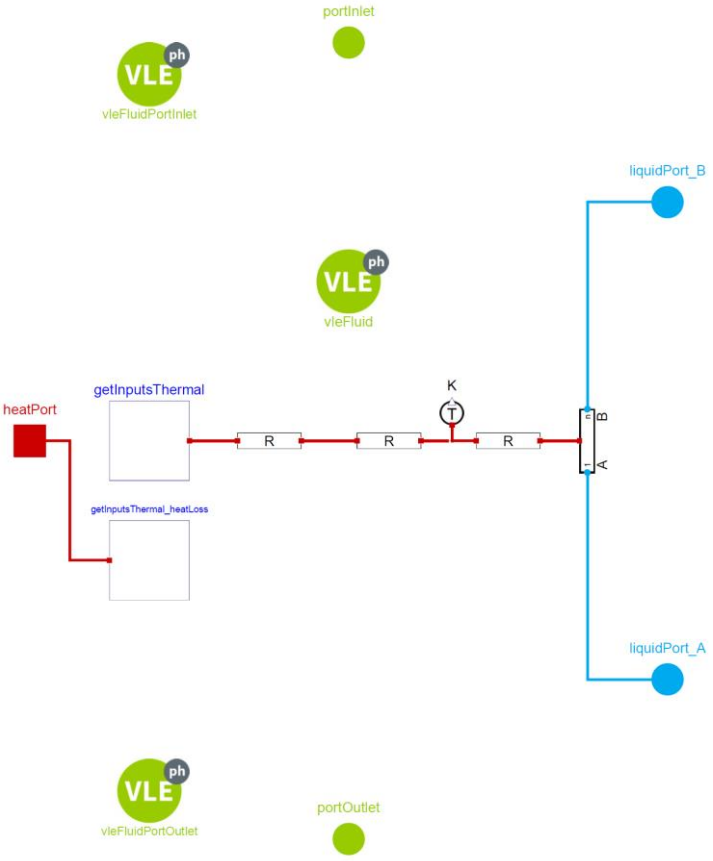

Figure 1. The overall schematic of the developed model for the reactor.

In the model structure, two VLE fluid ports are included to manage the inlet and outlet of vapor, and two liquid ports are provided to allow HTF to enter and exit the reactor tubes. In addition, heat ports are incorporated to account for energy losses to the environment and heat transfer within the reactor. A lump-parameter approach is developed to model the system dynamically. The model is designed as a system of ordinary differential equations (ODEs), considering changes over time and not changes in space.

3.2 Control Volume of the Salt Hydrate

The control volume of the salt hydrate is considered the core of the reactor model, and the governing equations for its behavior are presented below.

Reaction kinetics

To predict the rates of chemical reactions, empirical equations presented by Stengler et al. for the dehydration and hydration processes have been used [6].

$$\frac{dX}{dt} = (1.38 \cdot 10^6) \cdot exp\left\{\frac{-75.7 \cdot 10^3}{R \cdot T}\right\} \cdot (1 - X) \cdot \left(1 - \frac{P_{Cond}}{P_{Deh}}\right)^{0.25} \quad (1)$$

$$\frac{dX}{dt} = (3.04 \cdot 10^{-5}) \cdot (1 - X) \cdot \left(T_{@P_{Evap}} - T\right)^{1.79} \quad (2)$$

where X represents the progress of the reaction, P_{Deh} is the pressure-dependent reaction temperature for the dehydration process, P_{Cond} is the condenser pressure, and R is the universal gas constant. The pressure-dependent reaction temperatures for the dehydration and hydration processes are also determined based on the following empirical relationships [6]:

$$log\left(\frac{P_{Deh}}{P_{Ref}}\right) = 14.69 - \frac{6.41 \cdot 10^3}{T} \quad (3)$$

$$log\left(\frac{P_{Hyd}}{P_{Ref}}\right) = 8.18 - \frac{3.19 \cdot 10^3}{T} \quad (4)$$

Mass Balance

The mass balance for a compressible reactive gas (steam) is expressed as follows:

$$\frac{dm_{H_2O}}{dt} = \dot{m}_{In} - \dot{m}_{Out} + \dot{m}_{React} \quad (5)$$

here, $\dot{m}_{In}$ and $\dot{m}_{Out}$ represent the mass flow rates of water vapor entering and leaving the reactor, respectively, and $\frac{dm_{H_2O}}{dt}$ denotes the rate of change of the mass of water absorbed or released in the hydrated salt structure. The total mass of water in the hydrated salt is calculated using the following equation:

$$m_{H_2O} = \rho_{H_2O} \cdot \varepsilon_{Salt} \cdot V_{Reactor} \quad (6)$$

where ρ_{H_2O} is the density of water vapor, $V_{Reactor}$ is the effective volume of the reactor, and ε_{Salt} is the porosity, which depends on the conversion rate of the reaction. Additionally, $\dot{m}_{React}$ represents the rate of water vapor absorption or release during the chemical reaction and is calculated using the following equation:

$$\dot{m}_{React} = n_{H_2O} \cdot M_{H_2O} \cdot \frac{dX}{dt} \quad (7)$$

here, n_{H_2O} is number of moles, and M_{H_2O} is molar mass of water.

Energy Balance

The dynamic energy balance equation for the control volume of the salt hydrate is expressed as follows:

$$\frac{d\left(\dot{m}_{H_2O} \cdot h_{H_2O} + \dot{m}_{Salt} \cdot h_{Salt}\right)}{dt} = \dot{m}_{In} \cdot h_{Out} - \dot{m}_{Out} \cdot h_{Out} + \dot{Q}_{Pipe} + \dot{Q}_{React} + \dot{Q}_{Loss} \quad (8)$$

here, $\dot{Q}_{React}$ represents the rate of heat generation or absorption due to the chemical reaction, which is determined using the following relationship:

$$\dot{Q}_{React} = -\frac{\dot{m}_{React}}{M_{H_2O}} \cdot \Delta H_R \quad (9)$$

Additionally, the thermodynamic properties and heat transfer behavior of the hydrated salt during the reaction process are obtained using the following equations [6]:

$$\varepsilon_{Salt} = \varepsilon_{SrBr_2} + h \cdot \left(\varepsilon_{SrBr_2.H_2O} - \varepsilon_{SrBr_2}\right) \quad (10)$$

$$\rho_{Salt} = \rho_{SrBr_2} + h \cdot \left(\rho_{SrBr_2.H_2O} - \rho_{SrBr_2}\right) \quad (11)$$

$$Cp_{Salt} = Cp_{SrBr_2} + h \cdot \left(Cp_{SrBr_2.H_2O} - Cp_{SrBr_2}\right) \quad (12)$$

$$K_{Eff} = K_{H_2O} + K_{Bulk} \quad (13)$$

where, h denotes the specific surface area of the hydrated salt, which is taken as X for the hydration process and $1 - X$ for the dehydration process [6]. The chemical and physical properties of $SrBr_2{\cdot}H_2O$ are provided in Table 1.

Table 1. The chemical and physical properties of $SrBr_2{\cdot}H_2O$ [6].

Parameter	Variable	Value	Unit
Bulk thermal conductivity	K_{Bulk}	0.4	$W/(m \cdot K)$
Density of $SrBr_2$	ρ_{SrBr_2}	4216	kg/m^3
Density of $SrBr_2{\cdot}H_2O$	$\rho_{SrBr_2.H_2O}$	3911	kg/m^3
Enthalpy of reaction	ΔH_R	71.98	kJ/mol
Entropy of reaction	ΔS_R	143.93	$J/(mol \cdot K)$
Porosity of $SrBr_2$	ε_{SrBr_2}	0.71	-
Porosity of $SrBr_2{\cdot}H_2O$	$\varepsilon_{SrBr_2.H_2O}$	0.66	-
Specific heat capacity of $SrBr_2$	Cp_{SrBr_2}	75.35	$J/(mol \cdot K)$
Specific heat capacity of $SrBr_2{\cdot}H_2O$	$Cp_{SrBr_2.H_2O}$	120.9	$J/(mol \cdot K)$

3.3 Control Volume of the HTF

The control volume of the HTF tube is modeled by the single-phase liquid flow model from the TIL library. This model includes dynamic mass, energy, and momentum balances. The internal pressure drop of the tube is neglected under operating conditions. The internal heat transfer within the fluid is defined using the Gnielinski and Dittus-Boelter correlations. On the other hand, the heat transfer between the fluid and the tube wall is modeled based on circular geometry and stainless-steel material properties. The geometric characteristics of the tube are given in Table 2.

Table 2. Geometric characteristics of the reactor [4].

Parameter	Value	Unit
Fin base thickness	2.2	mm
Maximum distance between two fins	10	mm
Outer diameter of the tube	17.2	mm
Total lateral area of the fins	1.206	m^2
Tube length	61.77	m
Tube wall thickness	2.3	mm

3.4 Thermal Resistances

Heat transfer between the control volumes is calculated based on the thermal resistances defined between them. The total equivalent thermal resistance is calculated using the following equation:

$$R_{Cond,Fin\ base} = \frac{\ln\left(\frac{r_{Out}}{r_{In}}\right)}{2\pi L K_{Al}} \quad (14)$$

$$R_{Conv,Fin} = \frac{1}{(30 + 15h) \cdot A_{Fin}} \tag{15}$$

$$R_{Cond,Salt} = \frac{th_{Salt}}{A_{Fin}.K_{Salt}} \tag{16}$$

$$R_{Total} = R_{Cond,Fin\ base} + R_{Conv,Fin+R_{Cond,Salt}} \tag{17}$$

3.5 SGTHT Model

The SGTHT system is modeled using the reactor model and other components provided in the TIL library. The overall structure of the system is depicted in Figure 2. The thermal efficiency of the system is calculated using the following equation:

$$\eta_{Th} = \frac{\int \dot{Q}_{Hyd}\, dt + \int \dot{Q}_{DH}\, dt}{\int \dot{Q}_{Deh}\, dt + \int \dot{Q}_{Evap}\, dt} \tag{18}$$

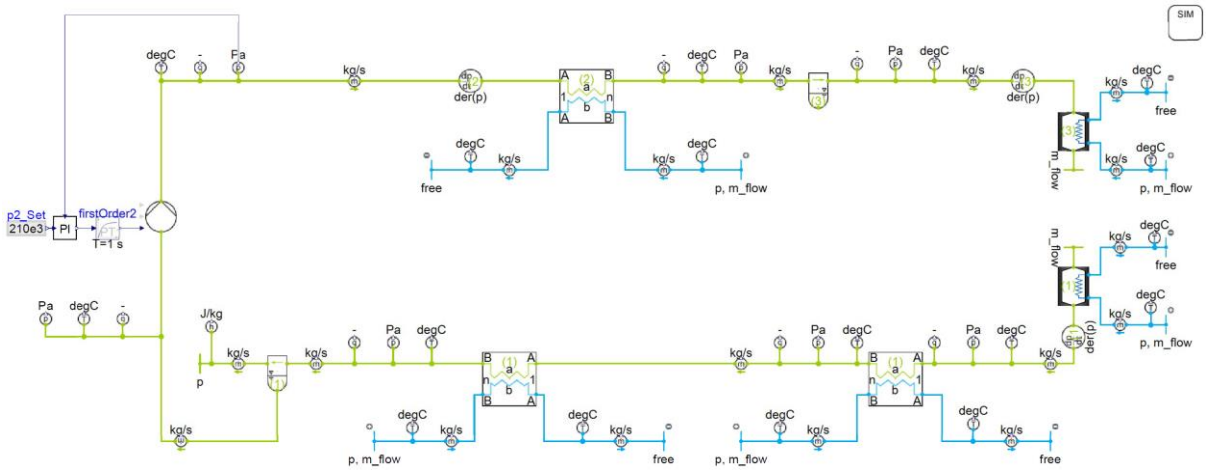

Figure 2. The overall model of the SGTHT system is implemented in the Dymola simulation environment.

The design conditions of the SGTHT system are provided in Table 3.

Table 3. Design and operational conditions of the SGTHT system.

Parameter	Value	Unit
Ambient pressure	101.3	kPa
Ambient temperature	25	℃
Condenser pressure	5.0	kPa
Evaporator pressure	210.0	kPa
Initial dehydration temperature	200.0	℃
Initial hydration temperature	200.0	℃
Reference pressure	1.0	kPa
Universal gas constant	8.314	$kJ/mol \cdot K$
Upgrade heat stream mass flow rate	10.2	kg/min
Waste heat stream mass flow rate	150.0	kg/min

4 Validation

The dynamic reactor model is developed based on the empirical model tested by Stengler et al. [6]. This model incorporates 5.059 kg of $SrBr_2 \cdot H_2O$. During the dehydration and hydration processes, the vapor pressures are 1.3 kPa and 66 kPa, respectively. The heat transfer fluid enters the

reactor at 189 °C with a mass flow rate of 16.4 kg/min during dehydration, and at 208 °C with a mass flow rate of 14.4 kg/min during hydration.

The results obtained from the developed dynamic model are presented in Figures 3–5 and compared with experimental data. The validation shows that the proposed dynamic model has a good agreement with experimental data. However, some deviations are observed. The primary source of these errors is related to the lumped modeling approach, which neglects space changes and considers only time changes. As a next step, a one-dimensional version of the dynamic model will be developed to enhance the accuracy of the results.

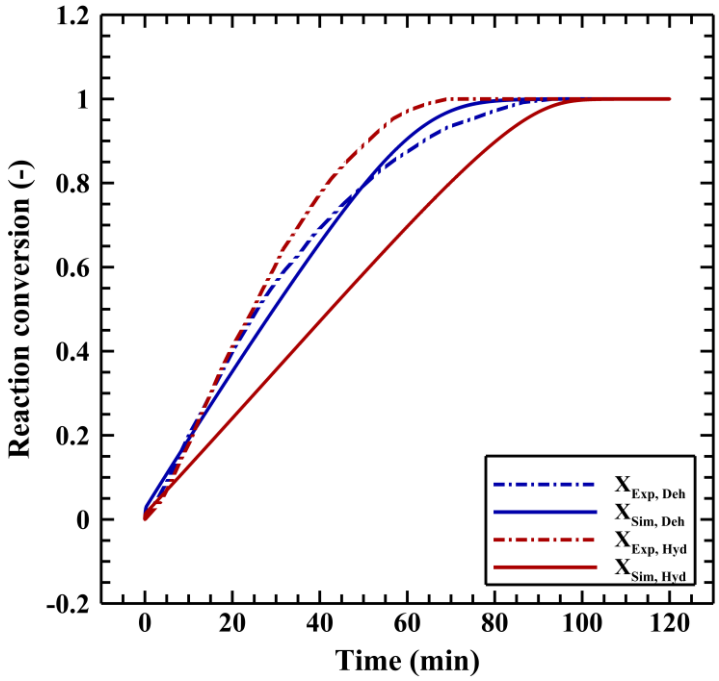

Figure 3. Comparison of the temporal profiles of reaction conversion based on experimental data and simulation outcomes for the SGTHT system.

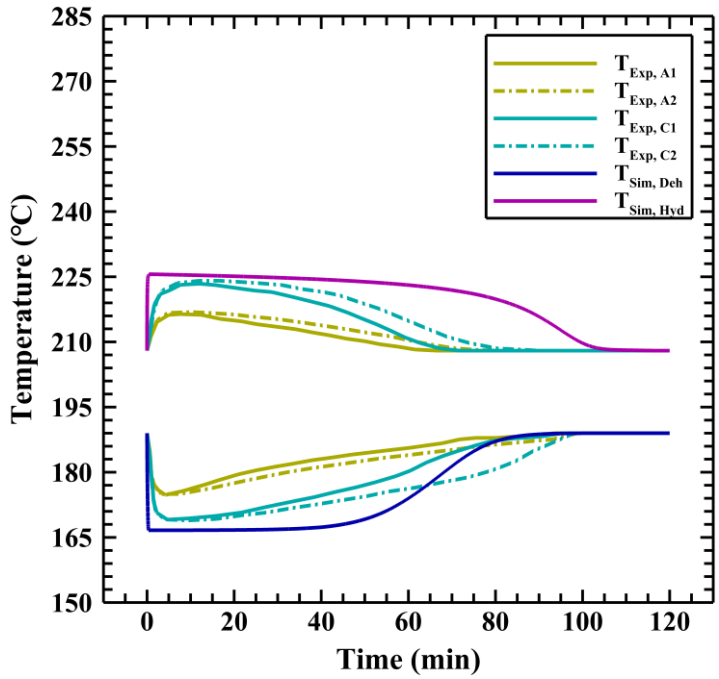

Figure 4. Comparison of the temporal profiles of salt temperature based on experimental data and simulation outcomes for the SGTHT system.

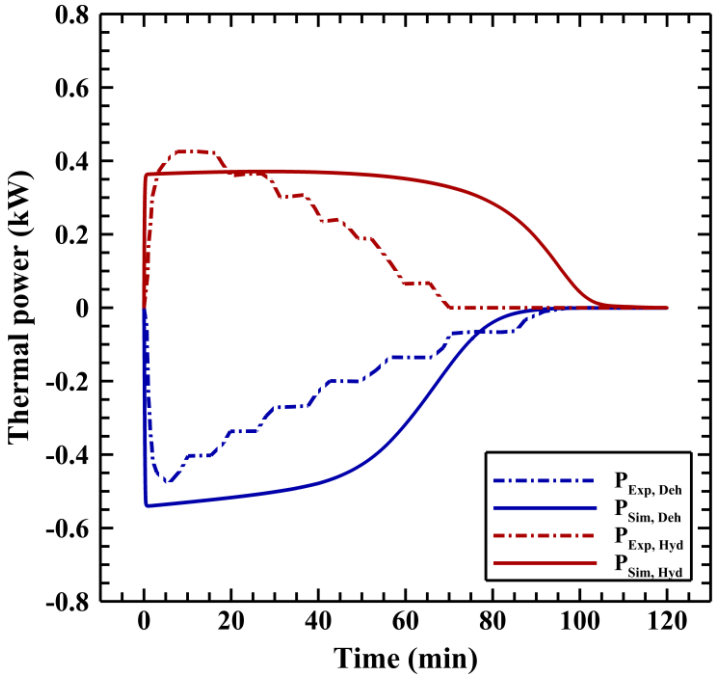

Figure 5. Comparison of the temporal profiles of system thermal power based on experimental data and simulation outcomes for the SGTHT system.

5 Results and Discussion

The SGTHT system is dynamically analyzed using the TIL library, the developed reactor model, and the design conditions presented in Table 3. To complete the dehydration and hydration processes within a two-hour period, the mass flow rates of HTF in the respective reactors are determined to be 150 kg/min and 10.2 kg/min, respectively. The variations in salt and HTF temperatures during the process are illustrated in Figure 6. Based on these results, the maximum and minimum temperatures during the hydration and dehydration processes are found to be 185 and 266.84 °C, respectively.

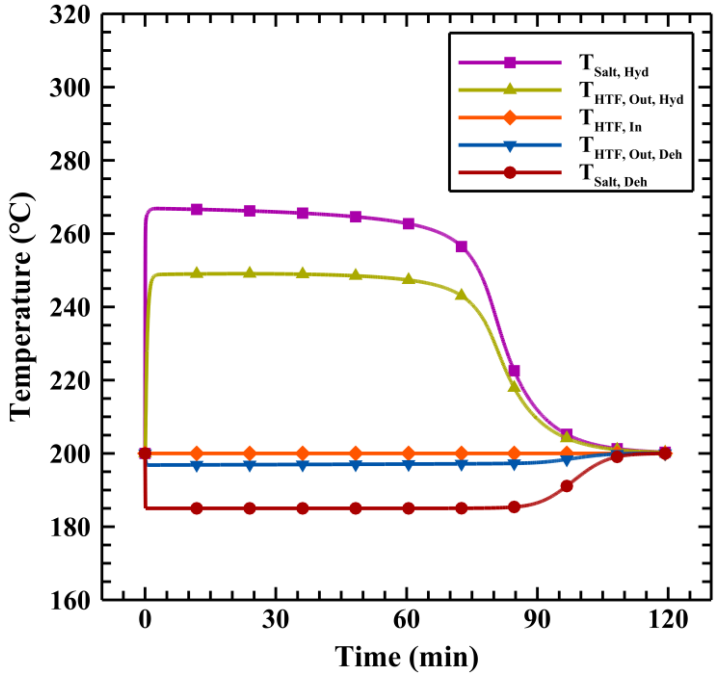

Figure 6. Temporal variation of salt and heat transfer fluid (HTF) temperatures during the dehydration (Deh) and hydration (Hyd) processes.

In the hydration reactor, the maximum temperature lift is 49.05 °C when the HTF mass flow rate is known. Since the salt temperature during the dehydration and hydration process depends on the condensation and evaporation pressures, the heat upgrading and recovery processes could be controlled by adjusting the vapor pressure. However, some limitations occur in the dehydration process where the vapor pressure is affected by the condenser temperature and cooling fluid temperature. In this study, the condensed vapor pressure is set at 5 kPa and the ambient temperature is assumed to be 25°C, corresponding to the saturation temperature of 32.86°C. More vapor pressure reduction leads to increased condenser dimensions and increased mass flow rate of cooling fluid.

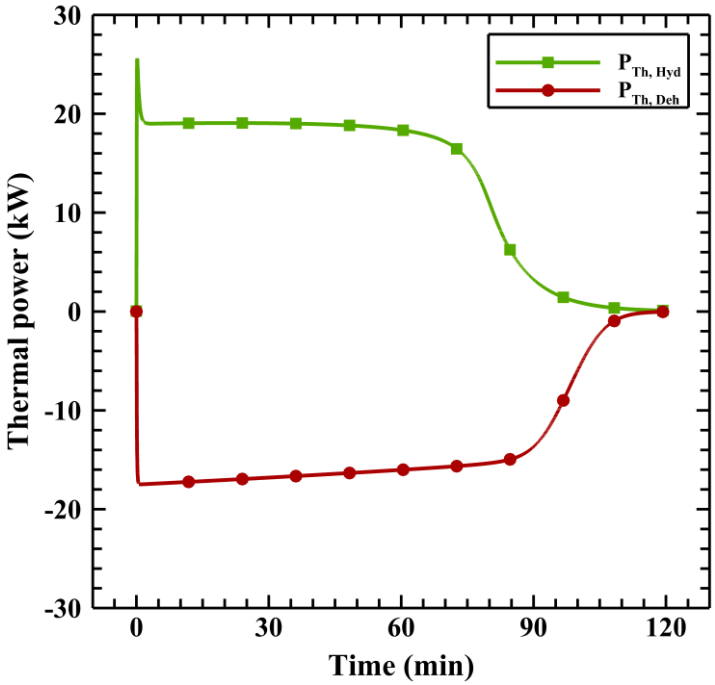

Figure 7. Temporal variation of system thermal power during the dehydration (Deh) and hydration (Hyd) processes.

The thermal power profile of the system during the dehydration and hydration processes is shown in Figure 7. According to Figure 7, the maximum heat transfer rates during these two processes are 17.49 and 25.61 kW, respectively. In the hydration process, a sudden spike in thermal power is observed at the beginning of the reaction, which is related to the limitations of the empirical equations provided in Ref. [6]. These equations are accurate only when the reaction conversion is between 10% and 80%. Outside this range, the model does not perform well. This issue is shown in Figures 8 and 9, which display the mass flow rate of water vapor released during dehydration and absorbed during hydration. At the beginning of the reaction, there is a sharp drop in mass flow rate, causing instability in the dynamic model.

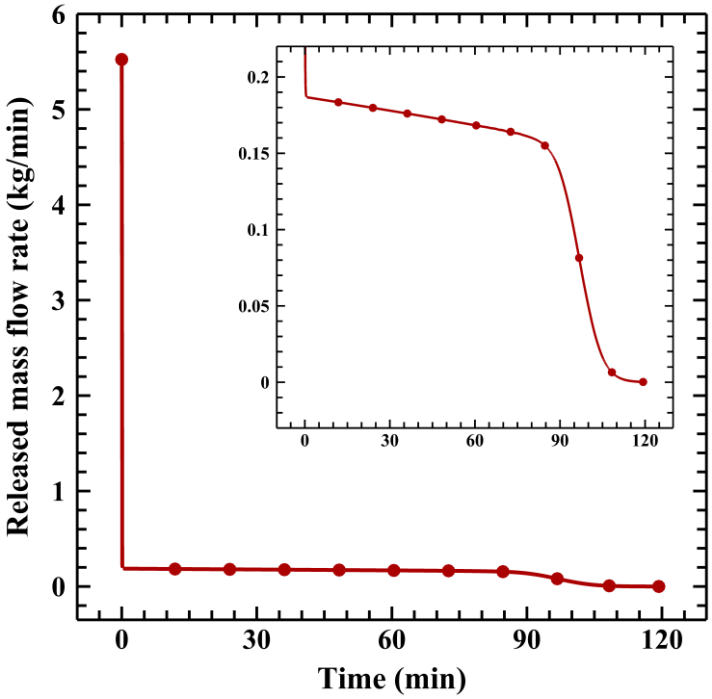

Figure 8. Temporal variation of released steam mass flow rate during the dehydration process.

The heat exchangers are designed based on the amount of water vapor flowing when the reaction reaches between 10% and 80% completion to keep costs low. Separators are placed at the outlets of these units, which can cause delays and changes in how the system responds.

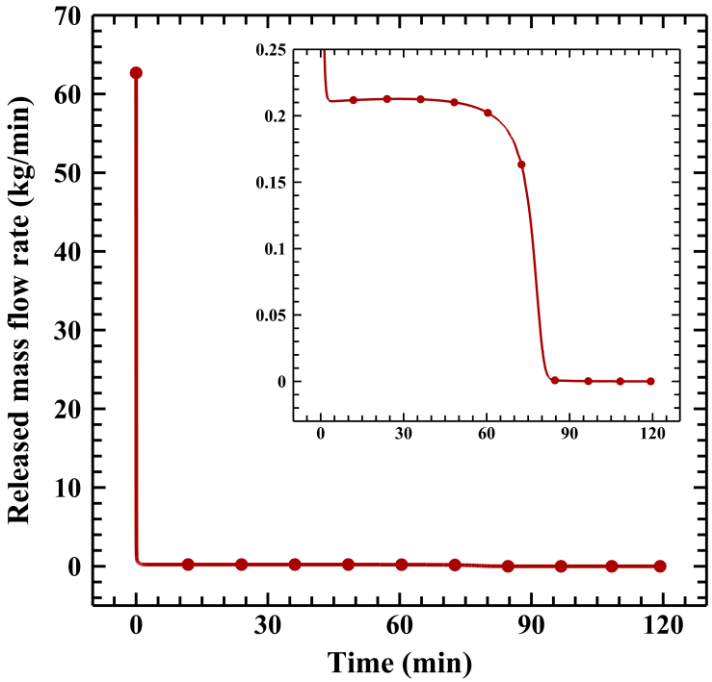

Figure 9. Temporal variation of absorbed steam mass flow rate during the hydration process.

The amount of heat transfer in the various components of the system is illustrated in Figure 10. During the process, the system absorbs 39.34 kWh of waste heat through the dehydration and evaporation processes and produces 25.94 kWh of upgraded heat via the hydration process. The steam from the dehydration reactor is very hot, so we use a heat exchanger before the condenser. This heat exchanger could be connected to a district heating network. The

results show that this heat exchanger can generate 1.33 kWh of heat at 80 °C, which could be used for district heating applications. The system's overall thermal efficiency is 69.34%.

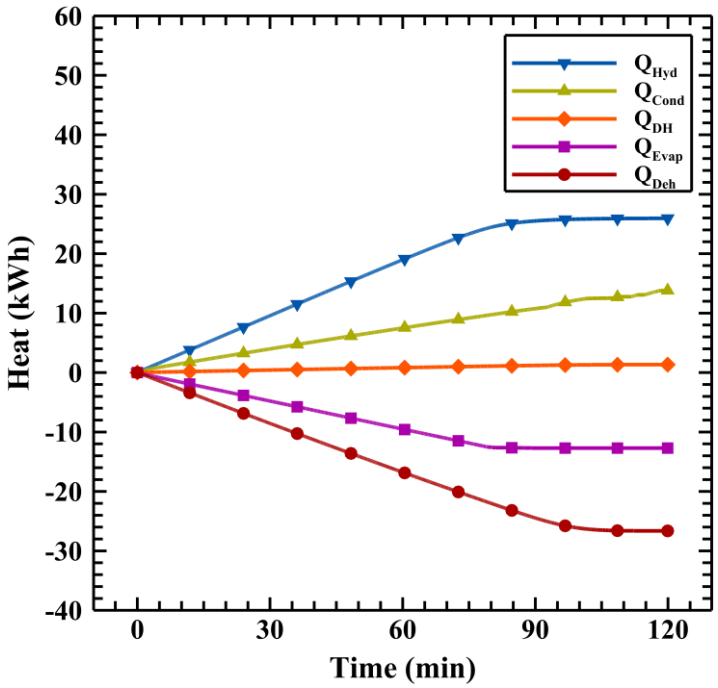

Figure 10. Heat transfer distribution among system components (including the hydration reactor, condenser, district heating via heat exchanger, evaporator, and dehydration reactor) as the process progresses over time.

The Van't Hoff diagram of the system is presented in Figure 11. This diagram is constructed under equilibrium conditions and includes three equilibrium lines corresponding to the dehydration process, the hydration process, and the water vapor–liquid equilibrium. Based on Figure 11, the theoretical temperature increase is 81.84 °C.

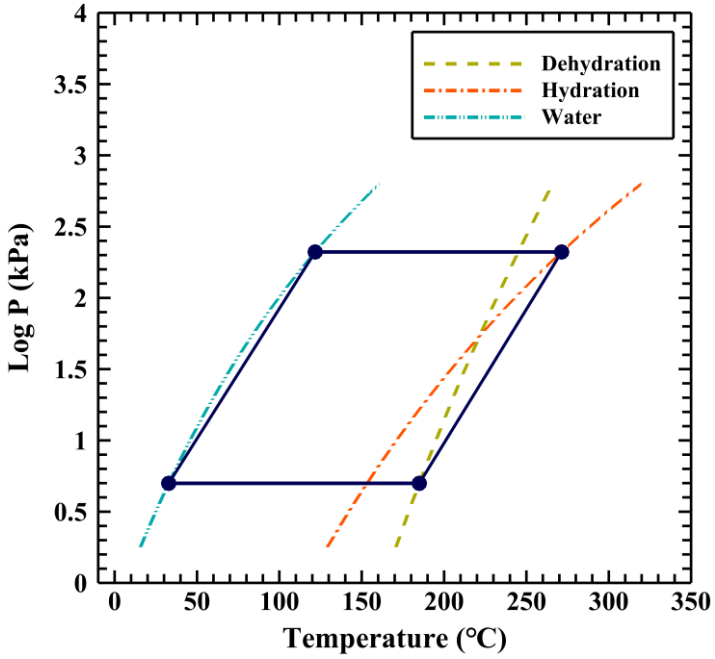

Figure 11. The Van't Hoff diagram of the SGTHT system.

6 Conclusion

A dynamic model of the SGTHT system is created using the Modelica language in the Dymola environment. The simulation results show that the system can upgrade waste heat from 200 °C to 249.05 °C using 250 kg of hydrated salt ($SrBr_2 \cdot H_2O$). Under these conditions, the overall thermal efficiency of the system is 69.34%. Furthermore, the model shows that some parameters, such as condensation and evaporation pressure, as well as HTF mass flow rate, have a significant impact on the performance of the system. To address the limitations observed in the reactor's dynamic behavior, a one-dimensional model will be developed. The current model is a lumped-parameter model, which assumes uniform properties throughout the reactor and considers only time variations, neglecting space changes.

7 Bibliography

[1] Hayatina I, Auckaili A, Farid M. Review on Salt Hydrate Thermochemical Heat Transformer. Energies 2023, Vol 16, Page 4668 2023;16:4668. https://doi.org/10.3390/EN16124668.

[2] Malleswararao K, Bürger I, Mejia AC, Kim ST, Linder M. Salt hydrate based thermochemical systems cascaded with high temperature mechanical heat pumps for waste heat recovery. Energy Conversion and Management: X 2024;24:100806. https://doi.org/10.1016/J.ECMX.2024.100806.

[3] Michel B, Dufour N, Börtlein C, Zoude C, Prud'homme E, Gremillard L, et al. First experimental characterization of CaCl2 coated heat exchanger for thermochemical heat transformer applications in industrial waste heat recovery. Appl Therm Eng 2023;227:120400. https://doi.org/10.1016/J.APPLTHERMALENG.2023.120400.

[4] Stengler J, Linder M. Thermal energy storage combined with a temperature boost: An underestimated feature of thermochemical systems. Appl Energy 2020;262:114530. https://doi.org/10.1016/J.APENERGY.2020.114530.

[5] Stengler J, Bürger I, Linder M. Thermodynamic and kinetic investigations of the SrBr2 hydration and dehydration reactions for thermochemical energy storage and heat transformation. Appl Energy 2020;277:115432. https://doi.org/10.1016/J.APENERGY.2020.115432.

[6] Stengler J, Bürger I, Linder M. Performance analysis of a gas-solid thermochemical energy storage using numerical and experimental methods. Int J Heat Mass Transf 2021;167:120797. https://doi.org/10.1016/J.IJHEATMASSTRANSFER.2020.120797.

[7] Michel B, Clausse M. Design of thermochemical heat transformer for waste heat recovery: Methodology for reactive pairs screening and dynamic aspect consideration. Energy 2020;211:118042. https://doi.org/10.1016/J.ENERGY.2020.118042.

Tech UPGRADE

CONTACT US

techupgrade.eu

FOLLOW US

Funded by the European Union

This project has received funding from European Union's Horizon Europe's Research and Innovation Program under grant agreement No. 101103966. Views and opinions expressed are however those of the author(s) only and do not necessarily reflect those of the European Union or the European Climate, Infrastructure and Environment Executive Agency (CINEA). Neither the European Union nor the granting authority can be held responsible for them.